

**Low-energy electron scattering from atomic hydrogen. I. Ionization**

J. G. Childers and K. E. James, Jr.

*Department of Physics, California State University, Fullerton, California 92834, USA*

Igor Bray

*Center for Atomic, Molecular and Surface Physics, School of Mathematical and Physical Sciences, Murdoch University, Perth 6150, Australia*

M. Baertschy

*Department of Physics, University of Colorado at Denver, Denver, Colorado 80217, USA*

M. A. Khakoo

*Department of Physics, California State University, Fullerton, California 92834, USA*

(Received 10 September 2003; published 23 February 2004)

Absolute doubly differential cross sections for the ionization of atomic hydrogen by electron impact have been measured at energies ranging from near threshold to intermediate values. The measurements are normalized to the accurate differential cross section for the electron-impact excitation of the H  $1^2S \rightarrow 2^2S + 2^2P$  transition. These measurements were made possible through the use of a moveable target source which enables the collection of hydrogen energy loss spectra free of all backgrounds. The measurements cover the incident electron energy range of 14.6–40 eV and scattering angles from  $12^\circ$  to  $127^\circ$ , and are in very good agreement with the results of the latest theoretical models—the convergent close-coupling model and the exterior complex scaling model.

DOI: 10.1103/PhysRevA.69.022709

PACS number(s): 34.80.Bm

**I. INTRODUCTION**

Low-energy electron-impact ionization processes play a fundamental role in fields ranging from atmospheric physics and astrophysics to the more terrestrial plasma processing, microelectronics fabrication, and electric lighting. At the heart of all of these processes lies the three-body Coulomb problem with two outgoing electrons. The interaction of an electron with a hydrogen atom in the ground state leading to ionization,  $H + e^- \rightarrow H^+ + 2e^-$ , is the simplest example of this problem and has therefore attracted significant theoretical interest. This work has led to the development of two *ab initio* theoretical models: the convergent close-coupling (CCC) model of Bray and Stelbovics [1] and Bray and Fursa [2] and the more recent exterior complex scaling (ECS) model of Rescigno *et al.* [3]. Detailed comparison of these two calculations by Baertschy *et al.* [4] revealed that significant disagreement between these models existed at energies near the ionization threshold.

Because of their difficulty, few experimental measurements of the differential cross sections for the electron-impact ionization of atomic hydrogen have been performed. Currently available measurements in the literature are the absolute doubly differential cross-section (DDCS) measurements of Shyn [5] and the triply differential cross-section (TDCS) measurements of Röder *et al.* [6,7]. The ECS calculation shows better agreement with the relative TDCS measurements than does the CCC calculation; however, there are questions concerning the normalization of the 15.6-eV TDCS data. Both calculations suggest that the normalized measure-

ments are too large by a factor of 2 [8,9]. This discrepancy has prevented an absolute comparison between theory and experiment. There remains a need for absolute, reliable measurements of the differential cross section for *e*-H ionization. In this paper, which expands upon a paper published as a Rapid Communication [10], we present absolute measurements of the DDCS for *e*-H ionization at the low incident electron energies ( $E_0$ ) of 14.6, 15.6, 17.6, 20, 25, and 40 eV and scattering angles ( $\theta$ ) ranging from  $10^\circ$  to  $127^\circ$ . In a following paper [11], we will present measurements of the DCS for elastic scattering and excitation of the  $n=3$  and 4 levels of atomic hydrogen that were taken during and following these measurements.

**II. EXPERIMENTAL METHOD**

Our apparatus has been discussed previously (see [12] and the references therein), so only a brief summary follows. The atomic beam is directed into the interaction region by an outside-silvered glass capillary needle of 0.5 mm internal diameter and is made to cross a monochromatic beam of electrons from the electron gun of an electrostatic electron spectrometer in a conventional beam-beam configuration. Scattered electrons are detected by an electrostatic analyzer as a function of energy loss ( $E_L$ ) and scattering angle. The analyzer has an additional pupil placed at the focal point of a two-element lens before the entrance to the hemispherical analyzer. This restricts the depth of field of the instrument so that it observes electrons only from a small volume of the collision region close to the capillary needle (about a

5–6-mm region). The analyzer has a four-element zoom lens to enable it to transmit electrons over a wide range of kinetic energies with essentially constant efficiency. To determine the efficiency of the analyzer, we measure the spectrum of He at 31.7 eV incident electron energy and 90° scattering angle. At this energy, the He ionization continuum is flat within 10% according to the Wannier law and as observed by, e.g., Keenan *et al.* [13].

To reduce the production of secondary electrons from surfaces in the experiment, the collision region is left open (all previous shielding grids [12] were removed, but care is taken to maintain grounded potentials around the collision region). The incident electron beam is collimated by two exit apertures of 1 mm in diameter spaced 12 mm apart to produce a beam of pencil angle [full width at half maximum (FWHM)] of about 3°, and the output electron optics have been modified so that the filling factor of the electron beam is at maximum approximately 0.5. The inside of all electron optics lenses is sprayed with colloidal graphite. We note that soot is significantly better and more stable at reducing secondary electrons than graphite, but has the minor disadvantage of causing electrical shorts between lenses. While these shorts can often be removed by “burning” them off using a high-voltage ( $\sim 300$  V) dc power supply, we found graphite both adequate in this location and significantly easier to apply. Finally, all surfaces around the collision region, including the analyzer nose cone and aperture assembly and the outside-silvered glass capillary needle, are liberally coated with soot from an acetylene flame. These steps succeeded in significantly reducing the number of slow background electrons remaining in the collision region.

The spectrometer performs with a typical incident electron current of  $\sim 50$ – $100$  nA with an energy resolution of about 120–150 meV (FWHM). This spectrometer has been proven to be stable over long periods ( $\sim 1$  year). The unit is baked at  $\approx 140$  °C to maintain stability against oil contamination. A separate heater is placed at the entrance of the electron analyzer to heat the real apertures at that location to  $\geq 150$  °C to keep them especially oil free since electrons travel through these apertures at the extremely low residual kinetic energies ( $E_1 = E_0 - E_L$ ) of  $0.5 \text{ eV} < E_1 < 10 \text{ eV}$ . This heating results in stable analyzer transmission during operation. The spectrometer is enclosed in a double  $\mu$ -metal shield to reduce the Earth’s magnetic field to less than 5 mG. The data acquisition and control system is computerized (angle settings, multichannel sweep, pressure monitoring, etc.), thus allowing for the continuous, overnight collection of data.

Our atomic H source, detailed in Paolini and Khakoo [14], is a recently developed extended cavity microwave discharge of 99.999%-purity H<sub>2</sub> operating at 2450 MHz. In general operation, the microwave power used is  $< 40$  W with a reflected power of 1–4 W. We prefer operating with this higher reflected power since in that configuration the center coax rod of the extended cavity ends about 4 mm from the quartz glass tube. This reduces the local power heating of the tube in the vicinity of the end of the rod which results in a lengthening of the tube’s lifetime [14]. The higher reflectance does not affect the dissociation fraction in the

discharge, and we are able to operate a single tube for periods as long as 2–3 months. Teflon tubing is used to conduct the atoms from the discharge tube to the outside-silvered glass needle. This source delivers an intense and stable H beam with a dissociation fraction of approximately 82%–85%.

Our measurements are comprised of electron energy loss spectra covering the  $E_L$  range from 6.5 eV to  $E_0 + 1$  eV. This covers the molecular hydrogen  $b^3\Sigma_u^+$  continuum plus the full range of H<sub>2</sub> excited states including the ionization continuum of H<sub>2</sub> starting at 15.94 eV [15]. This range also covers the entire energy loss spectrum of atomic hydrogen. A major difficulty in these experiments is the isolation of the atomic-hydrogen-related scattering signal from the combined backgrounds of molecular hydrogen scattering and secondary electrons. To determine the background contribution to the scattered electron signal due to secondary electrons, we initially tried the conventional “chopper” design in which a modulating flag is placed between the target gas beam and the collision region. This additional flag in the interaction region, however, was observed to generate a secondary source of scattered electrons, especially in the low-kinetic-energy region, that could not be distinguished from the continuum. We therefore discarded the flag and instead developed a movable source technique detailed in Hughes *et al.* [16]. In brief, the capillary needle is rotated so that the gas beam is pointed into (the “in” position) and away from (the “out” position) the collision region using a compact “Hobby-Shack” servomotor mounted to the needle. The motor is enclosed in a vacuum-tight box and the motor shaft is sealed from the experimental chamber using a single Viton o-ring. A spectrum measured with the needle in the “in” position contains contributions from gas-related scattering, scattering from background gas, and secondary electrons, whereas a spectrum measured with the needle in the “out” position contains only the contributions from scattering from background gas and secondary electrons. A simple subtraction of the “out” spectrum from the corresponding “in” spectrum therefore leaves a spectrum containing only the contribution from gas-related scattering. Using this method, excellent background determination free from additional electrons is observed for energies up to threshold. As a precaution, we verified that the needle in the “in” position did not serve as an additional source of secondary electrons by measuring spectra with no gas flowing through the needle. In this case, the measured “in” and “out” spectra differed by at most 0.5% at the lowest residual electron energies and significantly less than that at higher energies. This indicates that the needle did not contribute additional secondary electrons. To prevent an intermittent magnetic field produced by the electric current during motor operation from affecting the electron beam during data collection, it was switched off after reaching either position using a relay system operated by a one-shot LM555 integrated circuit. The servomotor is located well away from the electron beam path so that the small permanent magnetic field of the motor (measured to be  $< 2$  mG at a distance of 2 cm from the vacuum-sealed aluminum box) does not affect the beam at any position of the spectrometer.

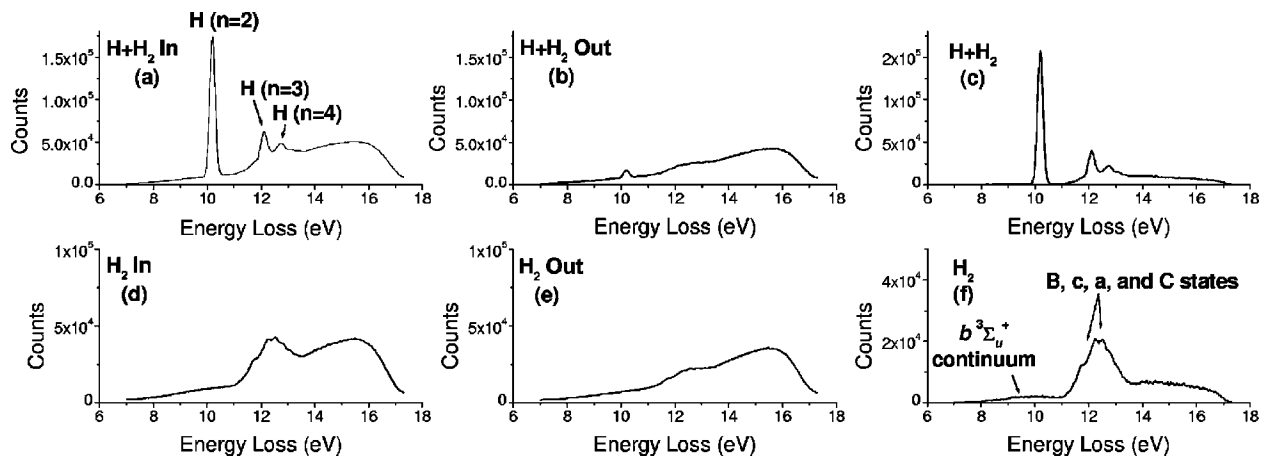


FIG. 1. (a) Electron energy loss spectrum taken at  $E_0=17.6$  eV and  $\theta=20^\circ$  with the discharge on and gas beam needle aligned with the electron beam. (b) Same as (a) but with gas beam needle displaced away from the electron beam (see text). (c) Spectrum in (b) subtracted from that in (a) without scaling. (d) Electron energy loss spectrum taken at  $E_0=17.6$  eV and  $\theta=20^\circ$  with the discharge off and gas beam needle aligned with the electron beam. (e) Same as (d) but with gas beam needle displaced away from the electron beam (see text). (f) Spectrum in (e) subtracted from that in (d) without scaling.

To obtain a single atomic H spectrum, electron energy loss spectra were measured with the microwave discharge source on and the gas needle cycling between the in and out positions every 3 min until good counting statistics were acquired. The microwave discharge source was then switched off and the experiment repeated, resulting in the collection of four spectra. These spectra were then analyzed as follows.

(i) The discharge on spectrum with gas beam out was subtracted from the corresponding discharge on spectrum with gas beam in. This resulted in an electron energy loss spectrum of a H+H<sub>2</sub> mixture with only gas-related scattering [Fig. 1(c)].

(ii) The discharge off spectrum with gas beam out was subtracted from the corresponding discharge off spectrum with gas beam in. This resulted in an electron energy loss spectrum of H<sub>2</sub> with only gas-related scattering [Fig. 1(f)].

(iii) The resultant H<sub>2</sub> spectrum in (ii) [Fig. 1(f)] was subtracted from the H+H<sub>2</sub> spectrum in (i) [Fig. 1(c)] after applying a scaling factor and allowing for small adjustments (<60 meV) for drifts along the energy loss scale. This scaled subtraction was critically determined (within 6% on average) by viewing the resultant spectrum and ensuring that there was no residual background in the energy loss region between the H( $n=2$ ), H( $n=3$ ), and H( $n=4$ ) energy loss features [compare Fig. 1(c) to Fig. 2]. Note that the adjustment for drifts in the energy loss scale, which enables us to optimize the residual background between the discrete H( $n$ ) peaks, does not affect the slowly varying ionization continuum.

The result of these subtractions is a pure spectrum of H consisting of discrete states resolved up to  $n=3$ , partially resolved  $n=4$ , and the continuum. To determine the transmission of the analyzer, following a series of measurements

of hydrogen spectra, a helium spectrum was measured using the same analyzer settings at  $E_0=31.7$  eV and  $\theta=90^\circ$ . As described previously, the He ionization continuum at this incident energy and angle is flat within 10%. This gives the analyzer transmission for residual electron energies up to  $\approx 7$  eV. This is sufficient for the transmission correction of the H spectra collected at  $E_0 \leq 20$  eV. At  $E_0=25$  and 40 eV, we extended the transmission correction to higher residual energies using the differential cross sections for He elastic scattering and excitation of the  $n=2, 3$ , and 4 levels from the CCC [17]. The transmission was found to be reproducible within <15%.

A typical resultant H spectrum following all corrections is shown in Fig. 2. Previous measurements [12,18] have shown

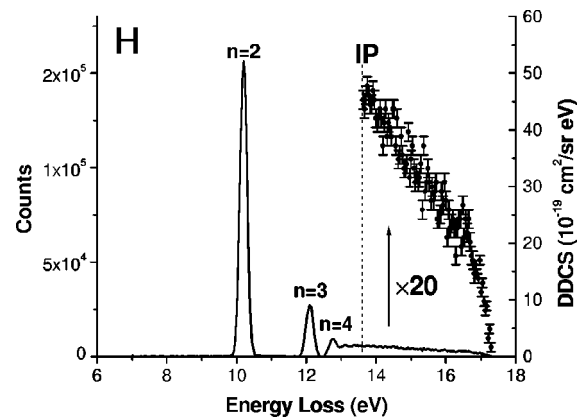


FIG. 2. Spectrum of H resulting from that in Fig. 1(f) subtracted from that in Fig. 1(c) using a scaling method (see text for details). IP labels the ionization potential. The continuum has been magnified by a factor of 20 and normalized as described in the text.

TABLE I. DDCS for the electron-impact ionization of H at  $E_0 = 14.6$  eV in units of  $10^{-19}$  cm<sup>2</sup>/sr eV. Those marked with an asterisk are measurements performed after the modification of the spectrometer. The quoted uncertainties are one standard deviation. See text for discussion.

Angle (deg)	$E_1$ (eV)	
	0.9	Uncertainty %
20	24.7	15.4
25	22.9	15.0
30	17.1	15.4
40	11.7	15.9
60	4.67	16.4
60*	5.77	19.9
90	2.85	16.0
90*	4	19.3
110	1.67	16.4
115*	2.2	19.3
127*	3.795	19.5

that the DCS for the excitation of the  $n=2$  level of H obtained from the CCC method [1,19] is accurate on the sub-10% level. Therefore, in place of the previous measurements themselves, the DCS obtained from the CCC method was used as the normalization standard to place our measurements of the continuum on an absolute scale. By fitting the continuum to a polynomial in energy loss of order  $\leq 4$ , we obtained the continuum doubly differential cross sections:

$$\frac{d^2\sigma(E_0, E_1, \theta)}{d\Omega dE} = \frac{N(E_1(\text{continuum}))}{N(n)\Delta E} \frac{d\sigma(n=2, E_0, \theta)}{d\Omega} \times \frac{\bar{T}(E_1(n=2))}{T(E_1(\text{continuum}))}, \quad (1)$$

where  $N(E_1(\text{continuum}))$  is the height of the continuum (number of electron scattering events) at position  $E_1$  in the continuum,  $\Delta E \approx 0.04$  eV is the energy step width per

TABLE II. DDCS for the electron-impact ionization of H at  $E_0 = 15.6$  eV in units of  $10^{-19}$  cm<sup>2</sup>/sr eV. The quoted uncertainties are one standard deviation. See text for discussion.

Angle (deg)	$E_1$ (eV)					Uncertainty %
	1.0	1.2	1.4	1.6	1.8	
15	31.6	34.3	37.2	40.5	44.0	16.7
20	33.8	35.4	37.0	38.3	39.7	16.1
25	35.1	35.0	34.6	33.9	33.0	17.8
30	19.1	18.0	17.3	17.0	17.1	16.5
40	9.69	11.2	12.2	12.6	12.5	15.8
60	5.17	5.44	5.64	5.77	5.83	16.5
90	3.00	3.05	3.09	3.14	3.19	16.7
120	4.69	4.98	5.22	5.42	5.56	31.7

TABLE III. DDCS for the electron-impact ionization of H at  $E_0 = 17.6$  eV in units of  $10^{-19}$  cm<sup>2</sup>/sr eV. The quoted uncertainties are one standard deviation. See text for discussion.

Angle (deg)	$E_1$ (eV)				Uncertainty %
	2.0	2.75	3.25	3.75	
12.5	18.2	27.7	34.6	41.8	17.0
15	17.2	25.6	31.1	36.4	16.1
17.5	16.0	22.4	27.6	33.6	15.9
20	14.1	19.4	23.8	28.8	16.0
30	12.3	14.7	16.1	17.5	16.5
40	7.04	7.93	8.33	8.62	17.5
60	3.45	3.56	3.70	3.89	16.9
90	2.10	2.29	2.39	2.57	18.4
110	2.75	2.84	2.89	2.95	18.1
120	2.89	3.21	3.42	3.61	18.2
125	4.24	4.34	4.47	4.70	16.4

channel,  $N(n)$  is the intensity (number of electron scattering events) under the H( $n=2$ ) energy loss line, and  $d\sigma(n=2, E_0, \theta)/d\Omega$  is the electron-impact excitation DCS for that level. The values  $T(E_1)$  are the analyzer transmission at  $E_1$  as determined by our He transmission runs. Error bars include statistical uncertainties propagated by all subtractions for both the continuum and discrete features, uncertainties in determining the subtraction parameters, uncertainties in transmission of the analyzer, and uncertainties in the polynomial fitting to the continuum. We do not assume any errors in the DCS for the H( $n=2$ ) feature from the CCC method.

### III. RESULTS AND DISCUSSION

Tables I–VI and the corresponding Figs. 3–10 contain our results. The  $E_0 = 14.6$  eV measurements are shown in Fig. 3. After the initial measurements were complete, we modified

TABLE IV. DDCS for the electron-impact ionization of H at  $E_0 = 20$  eV in units of  $10^{-19}$  cm<sup>2</sup>/sr eV. The quoted uncertainties are one standard deviation. See text for discussion.

Angle (deg)	$E_1$ (eV)					Uncertainty %
	2 <sup>a</sup>	3	4	5	6	
15	20.8	27.0	35.8	47.0	60.7	17.2
20	24.1	29.5	35.3	41.7	48.5	15.6
25	6.37	10.5	15.1	20.3	26.1	23.7
30	11.3	13.3	15.8	18.7	22.2	18.0
40	14.8	13.4	12.4	11.8	11.6	18.5
60	3.43	4.18	4.64	4.82	4.72	23.9
90	1.29	2.47	3.35	3.92	4.19	20.4
120	2.17	2.56	2.99	3.47	4.00	29.9

<sup>a</sup>Due to an increased uncertainty in the analyzer transmission at  $E_1 = 2$  eV, the overall uncertainty at this residual energy is  $\approx 5\%$  larger than at the higher residual energies.

TABLE V. DDCS for the electron-impact ionization of H at  $E_0=25$  eV in units of  $10^{-19}$  cm<sup>2</sup>/sr eV. The quoted uncertainties are one standard deviation. See text for discussion.

Angle (deg)	$E_1$ (eV)									Uncertainty %
	3 <sup>a</sup>	4	5	6	7	8	9	10	11	
12	14.9	16.1	20.1	27.0	36.9	49.6	65.2	83.8	105	17.5
14.5	11.4	10.6	12.7	17.8	25.9	36.9	50.8	67.7	87.6	19.9
17	14.1	16.5	20.4	25.7	32.5	40.7	50.4	61.5	74.0	16.3
20	9.46	10.9	13.2	16.7	22.5	27.9	34.4	42.1	51.1	16.7
27	15.8	15.0	14.6	14.8	15.4	16.5	18.1	20.2	22.7	24.0
30	3.91	4.66	5.72	7.15	9.50	11.5	13.9	16.6	19.7	17.2
37	4.18	4.35	4.67	5.15	5.79	6.58	7.53	8.64	9.91	41.6
40	4.06	4.53	5.01	5.54	6.45	6.87	7.35	7.92	8.55	18.1
60	3.73	3.79	3.80	3.82	4.07	4.00	3.99	4.06	4.20	16.1
90	3.38	3.38	3.33	3.26	3.38	3.21	3.09	3.03	3.02	16.3
110	3.70	3.61	3.47	3.30	3.31	3.05	2.85	2.72	2.66	19.7

<sup>a</sup>Due to an increased uncertainty in the analyzer transmission at  $E_1=3$  eV, the overall uncertainty at this residual energy is  $\approx 5\%$  larger than at the higher residual energies.

the spectrometer to extend the angular range to  $127^\circ$ . The measurements made after this modification are marked with an asterisk in Table I and shown as triangles in Fig. 3. Both sets of measurements agree very well with the calculations. This agreement is quite remarkable since this lowest incident energy presents the highest difficulty for both the calculations and experiment. In the measurements at higher incident energies presented below, the difficulty in determining the analyzer transmission at low residual energies will become evident. This measurement is the lowest, and therefore most difficult, residual energy measured in this series of experiments. We took significant effort and time to ensure that the transmission was correctly determined at this incident energy. The data at  $110^\circ$  and  $115^\circ$  appear to show a preference for the ECS calculation over the CCC calculation; however, we do not consider this conclusive.

At  $E_0=15.6$  eV, shown in Fig. 4, again the agreement is very good. The slight increase in the measurement above the calculations (about 30%–40%) at  $\theta=20^\circ$  and  $25^\circ$  may be due to either the increased difficulty in determining the analyzer transmission at lower residual energies or a small, un-

detected systematic error in the background subtraction procedure.

At  $E_0=17.6$  eV, shown in Fig. 5, we see perhaps the first sign of significant disagreement between our measurements and the calculations. Our measurements lie on average about 30% below the two calculations. We have investigated various sources of systematic error including, among others, poor grounding of the analyzer nose cone resulting in an accumulation of charge and sources of background electrons not accounted for in the data analysis, but could not find any such corrections. Also shown in Fig. 5 is the original CCC calculation. A comparison of the measured DDCS with the calculations facilitated the correction of a problem in the original calculation [20]. The corrected calculation, shown as the dotted line in all the figures, is now in much better agreement with the ECS calculation.

Figure 6 shows the measurements taken at  $E_0=20$  eV. We return to excellent agreement with the calculations. The increased difficulty in determining the analyzer transmission at low residual energies is evident here as an increased scatter in the measured values at lower residual energies. In

TABLE VI. DDCS for the electron-impact ionization of H at  $E_0=40$  eV in units of  $10^{-19}$  cm<sup>2</sup>/sr eV. The latter measurements are marked with an asterisk. The quoted uncertainties are one standard deviation. See text for discussion.

Angle (deg)	$E_1$ (eV)										Uncertainty %	
	2	3	5	7	10	13	15	17	20	23		26
10	10.8	9.82	9.03	8.63	8.74	9.69	11.8	17.0	37.1	85.5	186	17.8
10*	8.77	7.61	5.85	5.08	4.73							19.6
15	6.30	6.31	6.51	6.43	6.68	8.24	10.7	15.1	27.8	52.8	98.2	16.3
15*	6.30	5.73	5.18	5.74	7.06							15.5
20	7.15	6.25	4.85	3.90	4.05	5.89	8.00	11.0	17.9	29.8	50.1	16.4
30	4.21	4.14	4.04	3.81	3.96	4.91	5.96	7.28	9.71	12.5	15.3	16.0
60	3.73	3.67	3.53	3.13	2.61	2.31	2.18	2.07	1.96	1.92	2.07	20.2
90	3.44	3.47	3.40	2.95	2.21	1.64	1.36	1.17	1.01	0.964	0.945	18.3
110	4.58	4.28	3.60	2.69	1.65	1.07	0.861	0.741	0.656	0.615	0.595	18.1

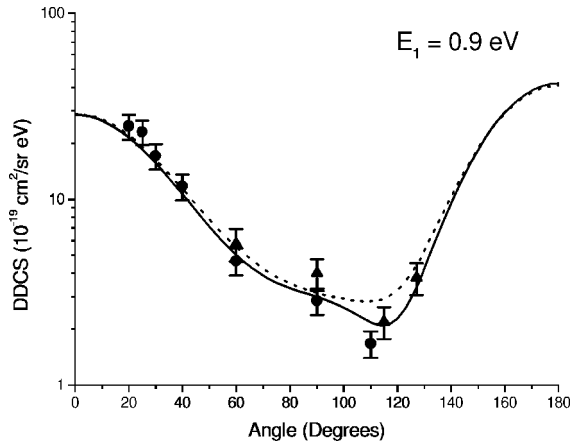


FIG. 3. Doubly differential cross section for the electron-impact ionization of H at  $E_0 = 14.6$  eV obtained from the present experiments (before  $\bullet$  and after  $\blacktriangle$  modification of the spectrometer) and compared to the ECS [9] (solid line) and CCC [20] (dotted line).

Table IV, we also present our measured DDCS at  $E_1 = 2$  eV. Because of the increased uncertainty in the analyzer transmission at this lower residual energy, the overall uncertainty is  $\approx 5\%$  larger than at the higher residual energies.

Figures 7 and 8 show the measurements taken at  $E_0 = 25$  eV. We continue to see excellent agreement with the

calculations. We also see excellent agreement with the measurements of Shyn [5] at  $E_1 = 6$  eV. The difficulty in determining the analyzer transmission at low residual energies is again evident. In Table V, we present our measured DDCS at  $E_1 = 3$  eV, but again the overall uncertainty at that residual energy is  $\approx 5\%$  larger than at the higher residual energies.

Finally, at  $E_0 = 40$  eV, shown in Figs. 9 and 10, we see excellent agreement with the calculations with the exception of low residual energies at forward scattering angles. Our measurements there, as at all other incident energies and residual energies, show a forward scattering peak that is absent in both of the calculations. To verify this disagreement with the calculations, we performed additional measurements at  $10^\circ$  and  $15^\circ$  scattering angles. These latter measurements, marked with an asterisk in Table VI and shown as triangles in Fig. 9, confirm the disagreement. Again, we searched for possible sources of systematic error and found none. At higher residual energies, especially at the highest  $E_1 = 26$  eV, the agreement with the calculations is outstanding. Also shown are the earlier measurements of Shyn which are in poorer agreement with the calculations.

#### IV. CONCLUSIONS

We have measured accurate DDCS's for the ionization of atomic H by electron impact at energies close to threshold.

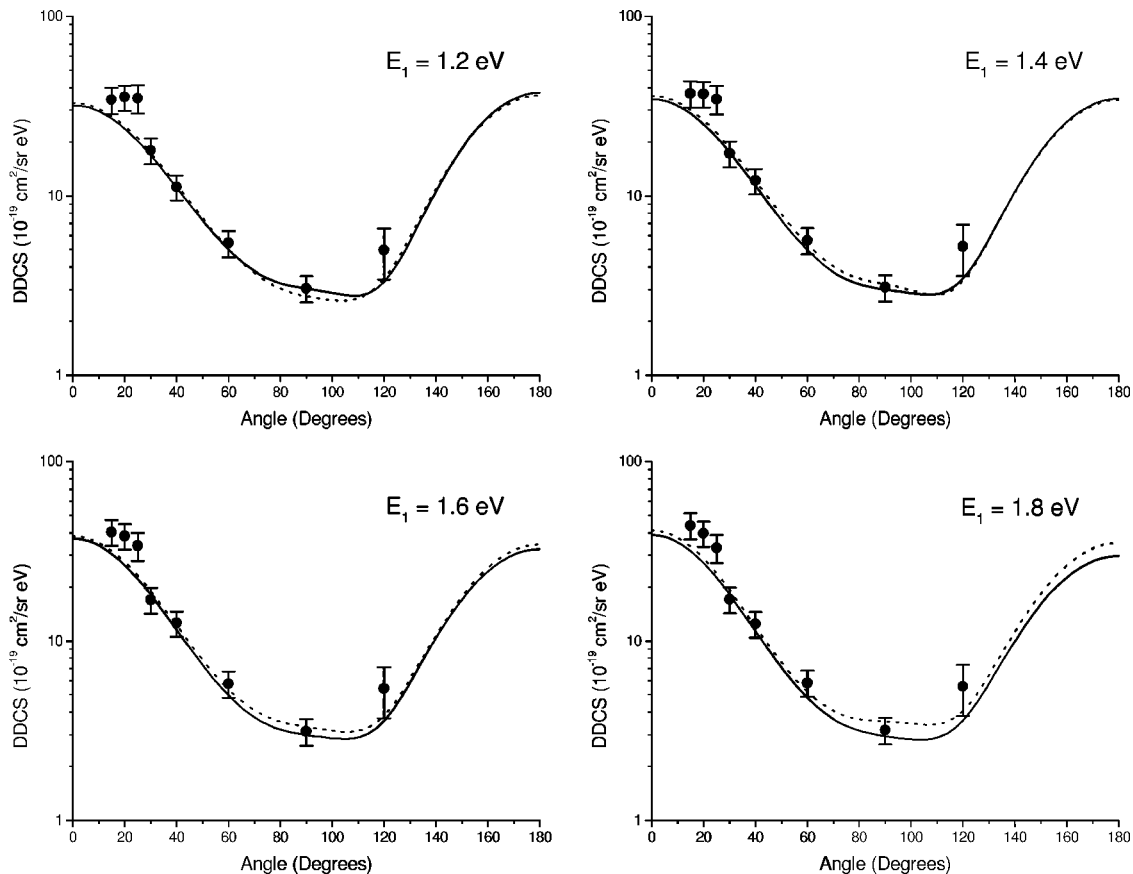


FIG. 4. Doubly differential cross sections for the electron-impact ionization of H at  $E_0 = 15.6$  eV obtained from the present experiments ( $\bullet$ ) and compared to the ECS [9] (solid lines) and the recent CCC [20] (dotted lines) shown for different  $E_1$  values.

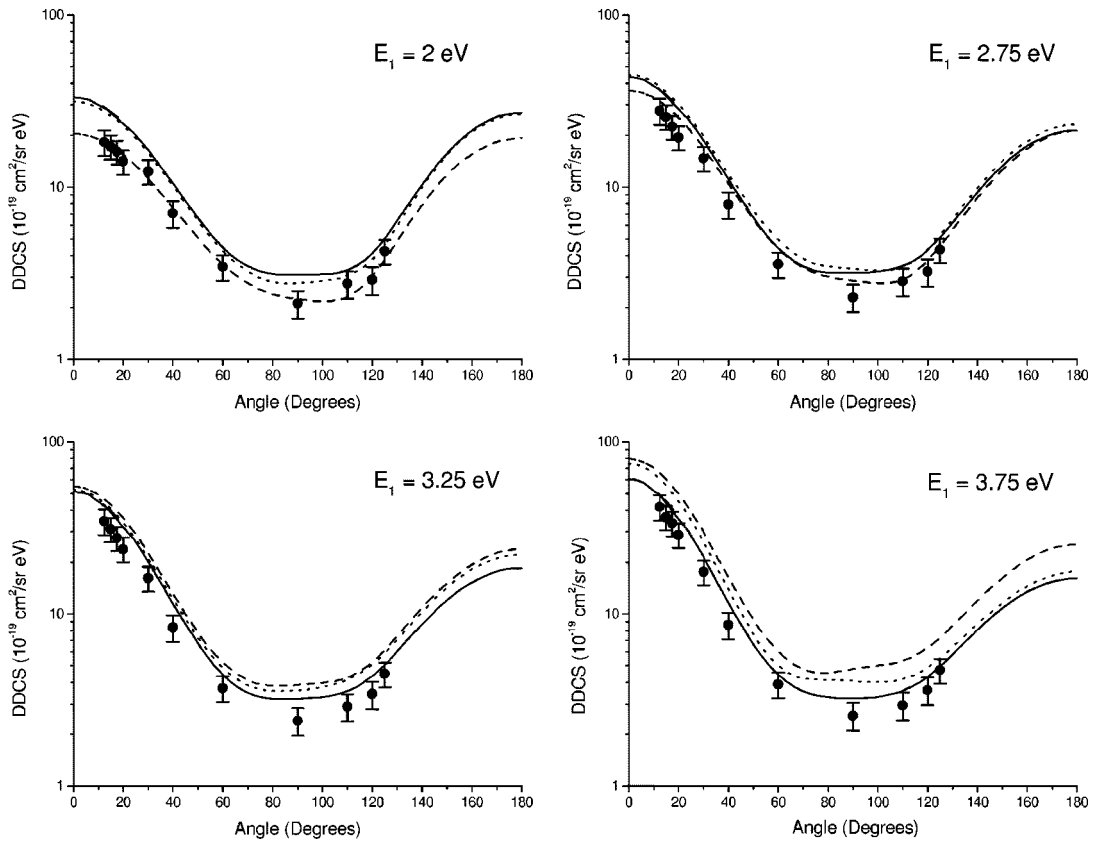


FIG. 5. Same as Fig. 4, but for  $E_0=17.6$  eV. Also shown is the earlier CCC calculation (dashed lines). See text for discussion.

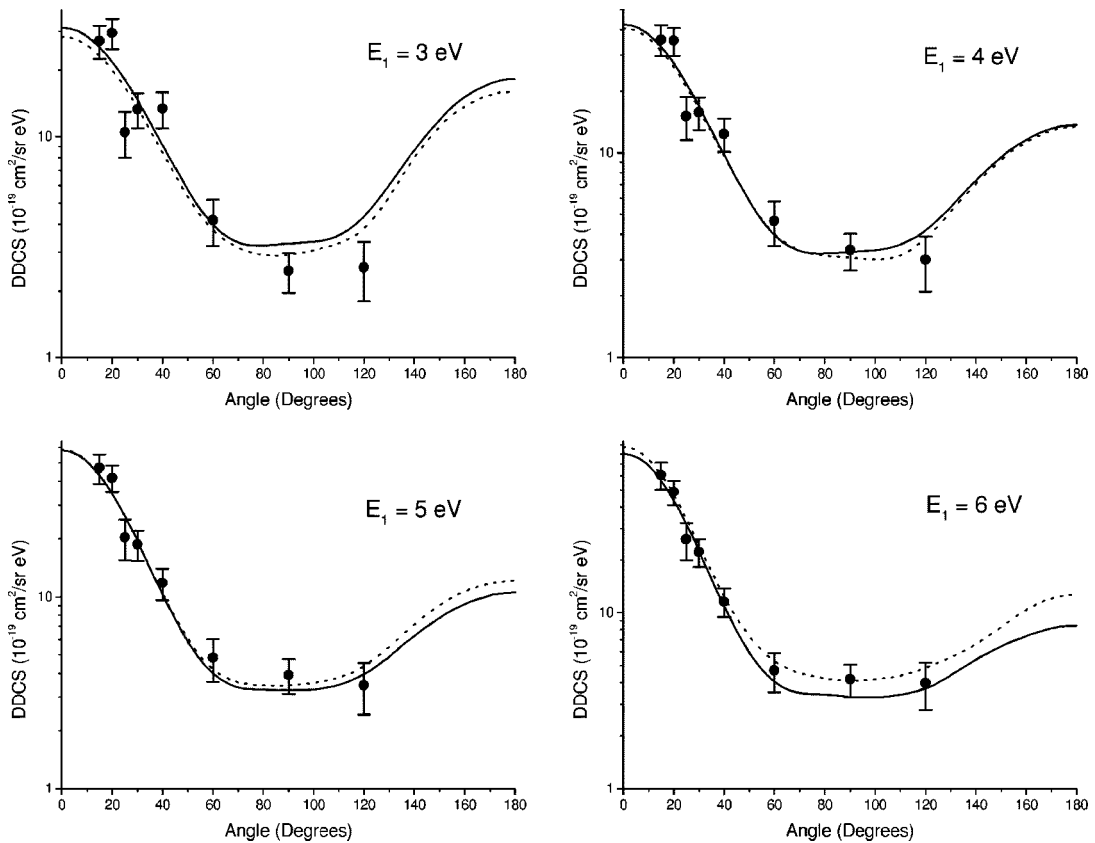


FIG. 6. Same as Fig. 4, but for  $E_0=20$  eV.

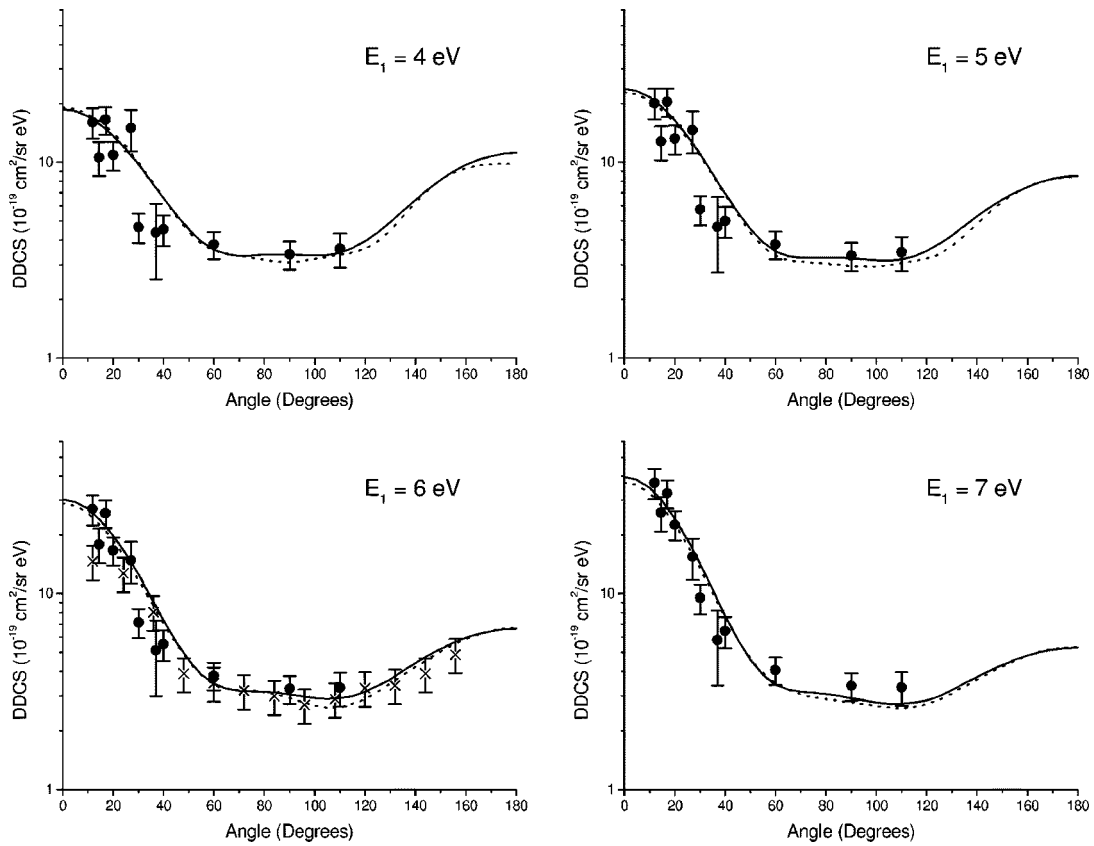


FIG. 7. Same as Fig. 4, but for  $E_0 = 25$  eV. Also shown are the measurements of Shyn [5] ( $\times$ ) where available.

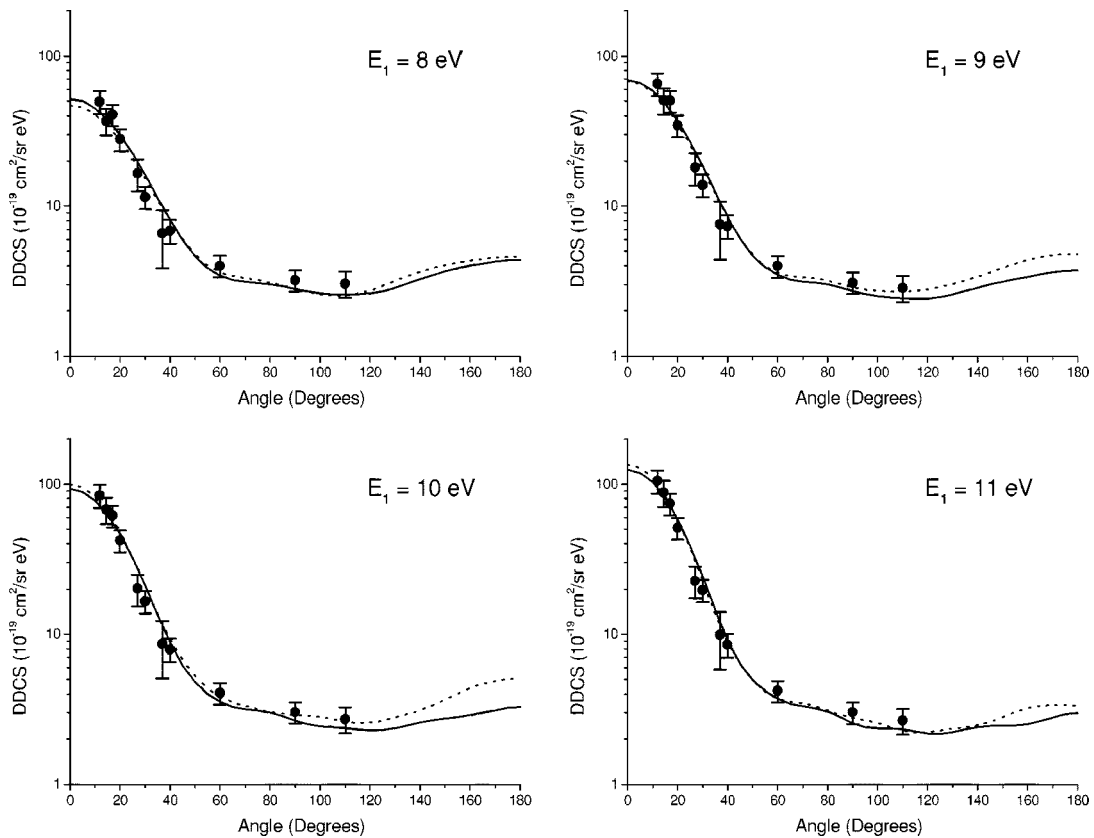


FIG. 8. Same as Fig. 7, but for higher  $E_1$  values.

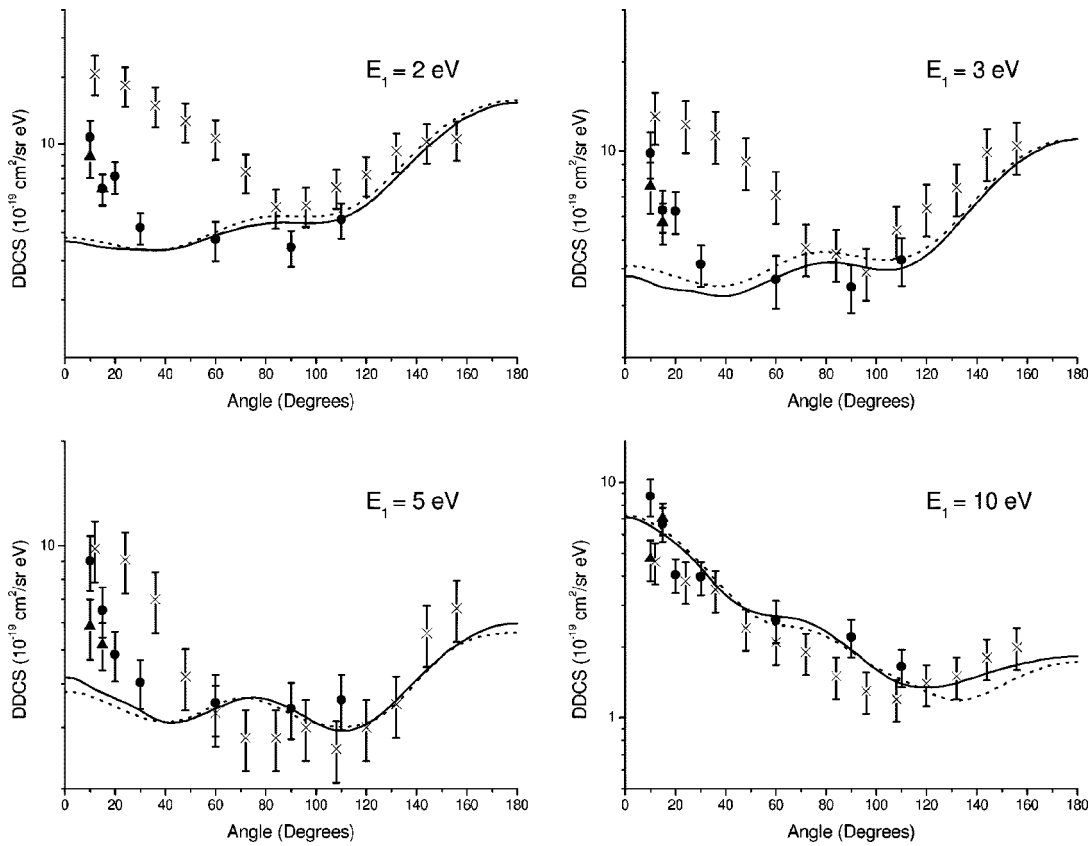


FIG. 9. Same as Fig. 4, but for  $E_0 = 40$  eV. Also shown are later measurements ( $\blacktriangle$ ) performed to verify the disagreement with the calculations at low residual energies.

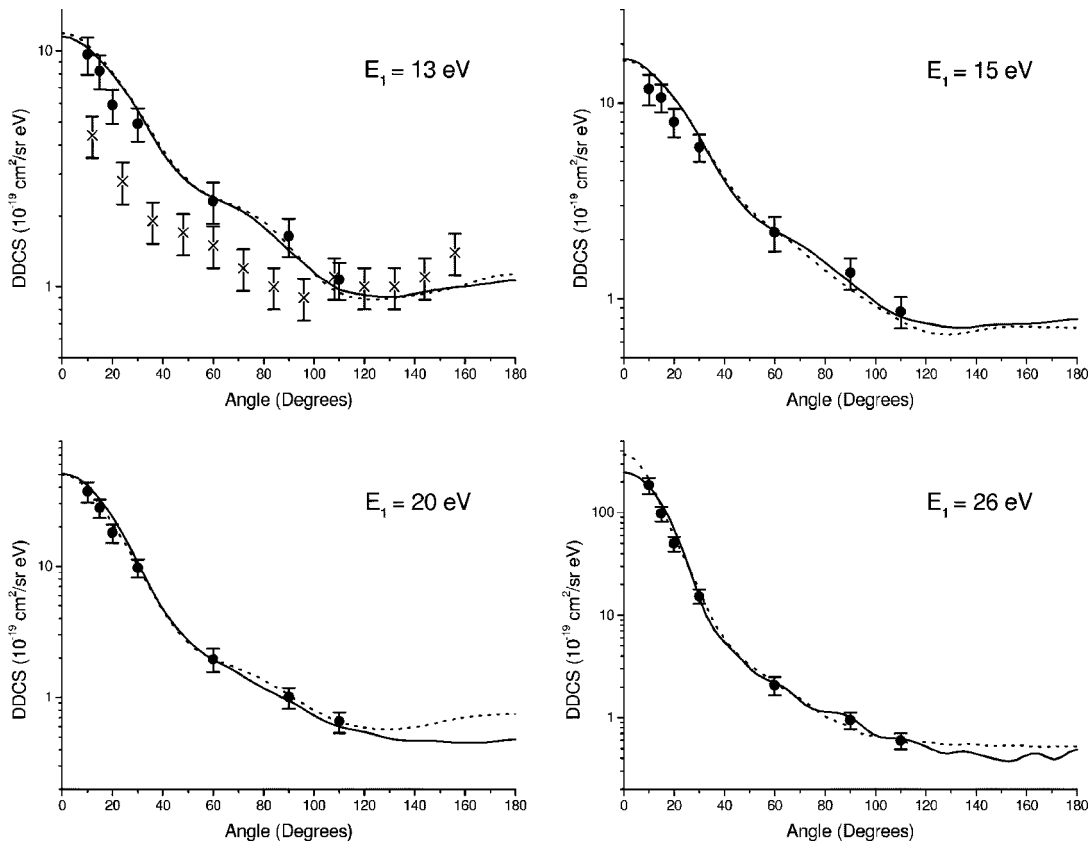


FIG. 10. Same as Fig. 9, but for higher  $E_1$  values.

These measurements were made possible by the use of a moveable H+H<sub>2</sub> source developed in our laboratory. We are able to obtain, after a relatively simple and direct data analysis, an energy loss spectrum of background-free H. These measurements facilitated an improvement of the CCC calculation, which is now in better agreement with our measurements and the ECS calculation. The results, however, do not show complete agreement with either of these calculations and suggest that the calculations may need to include more

channels to agree with our measurements at higher incident energies at small scattering angles.

#### ACKNOWLEDGMENTS

This project was funded by a grant from the National Science Foundation under Grant No. NSF-RUI-PHY-0096808. We acknowledge the expert help of technical staff Jorge Meyer (glass blowing shop), David Parsons (machine shop), and Hugo Fabris (electronics shop).

- 
- [1] I. Bray and A. Stelbovics, *Phys. Rev. A* **46**, 6995 (1992).  
[2] I. Bray and D.V. Fursa, *Phys. Rev. A* **54**, 2991 (1996).  
[3] T.N. Rescigno, M. Baertschy, W.A. Isaacs, and C.W. McCurdy, *Science* **286**, 2474 (1999).  
[4] M. Baertschy, T.N. Rescigno, W.A. Isaacs, X. Li, and C.W. McCurdy, *Phys. Rev. A* **63**, 022712 (2001).  
[5] T.W. Shyn, *Phys. Rev. A* **45**, 2951 (1992).  
[6] J. Röder, J. Rasch, K. Jung, C.T. Whelan, H. Ehrhardt, R.J. Allan, and H.R.J. Walters, *Phys. Rev. A* **53**, 225 (1996).  
[7] J. Röder, H. Ehrhardt, C. Pan, A.F. Starace, I. Bray, and D.V. Fursa, *Phys. Rev. Lett.* **79**, 1666 (1997).  
[8] I. Bray, *J. Phys. B* **32**, L119 (1999).  
[9] M. Baertschy, T.N. Rescigno, and C.W. McCurdy, *Phys. Rev. A* **64**, 022709 (2001).  
[10] J.G. Childers, K.E. James, Jr., M. Hughes, I. Bray, M. Baertschy, and M.A. Khakoo, *Phys. Rev. A* **68**, 030702(R) (2003).  
[11] K.E. James, Jr., J.G. Childers, and M.A. Khakoo, following paper, *Phys. Rev. A* **69**, 022710 (2004).  
[12] M.A. Khakoo, M. Larsen, B. Paolini, X. Guo, I. Bray, A. Stelbovics, I. Kanik, S. Trajmar, and G.K. James, *Phys. Rev. A* **61**, 012701 (1999).  
[13] G.A. Keenan, I.C. Walker, and D.F. Dance, *J. Phys. B* **15**, 2509 (1982).  
[14] B.P. Paolini and M.A. Khakoo, *Rev. Sci. Instrum.* **69**, 3132 (1998).  
[15] G. Herzberg, *Spectra of Diatomic Molecules* (Van Nostrand, New York, 1950).  
[16] M. Hughes, K.E. James, Jr., J.G. Childers, and M.A. Khakoo, *Meas. Sci. Technol.* **14**, 841 (2003).  
[17] D.V. Fursa and I. Bray, *Phys. Rev. A* **52**, 1279 (1995).  
[18] A. Grafe, C.J. Sweeney, and T.W. Shyn, *Phys. Rev. A* **63**, 052715 (2001).  
[19] I. Bray (private communication).  
[20] I. Bray, *Phys. Rev. Lett.* **89**, 273201 (2002).